Animal Models of Diabetic Complications Consortium
(U01 DK076160)

Annual Report
(2010)

"Mitochondrial SOD as a Target for Diabetic Neuropathy"

University of Michigan

Principal Investigator
Eva L. Feldman, M.D., Ph.D.

Address:
109 Zina Pitcher Road
5017 BSRB
Ann Arbor MI 48109-2200
Phone: (734) 763-7274
E-mail: efeldman@umich.edu

Table of Contents

Animal Models of Diabetic Complications Consortium
(U01 DK076160)

Part A:

Principal Investigator's Summary

1. Program Accomplishments:

Hypothesis:

We continue to investigate the damaging effects of diabetes-induced oxidative stress on the nervous system. Our primary goal is examining the onset and progression of diabetic polyneuropathy (DPN). Recent data collected from animal models of type 2 diabetes confirm our hypothesis that oxidative damage occurs in axons and that damaged axonal mitochondria contribute to the distal loss of axonal function which is the hallmark of DPN i.e. the idea of a stocking/glove neuropathy [1]. In order to better assess mitochondrial (Mt) biology in axons, we developed a novel technique to assess Mt fission and fusion and are currently applying this technique to *in vitro* models of DPN [2]. We also completed a careful examination of the effects of different commonly used anesthetics on our electrophysiological measures of mouse models of DPN; this assessment showed that isofluorane is the most appropriate anesthetic and this is now being used by us and our colleagues in mouse models of DPN [3].

At the suggestion of the EAC, we are exploring additional behavioral measurements of DPN, in particular pain. Our most recent data begin to explain the mechanisms underlying painful DPN in a type 2 mouse model [4]. Finally, at the suggestion of the EAC, we are continuing our work in the central nervous system of mouse models of diabetes, and report cortical neurons are damaged in a mouse model of type 2 diabetes [5]. The current results of these studies are detailed below.

Progress Towards Stated Milestones:

Mt Responses to Hyperglycemia *in vivo* and *in vitro*.

We explored the hypothesis that Mt oxidative stress in diabetes-induced hyperglycemia will induce a response to generate more Mt via fission and/or biogenesis. Initially, we exposed DRG neurons cultured from adult mice (non-diabetic, C57/Bl6) to control (5.7 mM) or high (25.7 mM) glucose for 6 and 24 h then examined Mt DNA and Mt gene expression (Fig. 1). We found that Mt DNA significantly increased over 24 h, suggesting that DRG neurons induce Mt biogenesis to process the elevated metabolic substrates (Fig. 1a). Next, we explored mRNA both for Mt encoded proteins and for transcription factors and other Mt regulatory proteins encoded in the Mt or nucleus. Transcription factors and the fission protein Fis1 were found to be elevated in hyperglycemia, which suggests that a combination of both biogenesis and fission are activated.

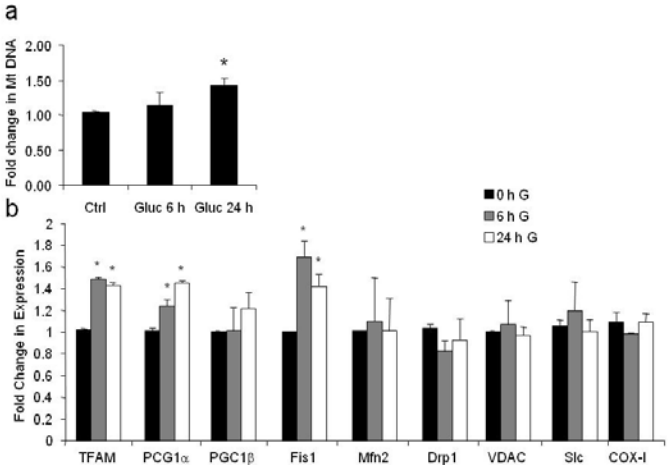

Figure 1. Increased Mt DNA and mRNA for Mt proteins in high glucose. DRG neurons from C57/Bl6 mice were exposed to 25.7 mM glucose for 0, 6, or 24 h, and then mRNA and DNA were isolated. In (a), MtDNA was normalized to the levels of nuclear DNA. *After 24 h hyperglycemia, there was a significant increase in MtDNA relative to nuclear DNA, $p<0.01$. . In (b), mRNA was subjected to quantitative RT-PCR for Mt transcription factors, fission and fusion proteins, and Mt functional proteins. *TFAM, PGC1α, and Fis1 were significantly increased after 6-24 h hyperglycemia, $p<0.01$.

Given *in vitro* data that Mt undergo increased biogenesis and fission in hyperglycemia, we returned to our mouse models of diabetic neuropathy to corroborate this finding *in vivo*. We performed nerve electron microscopy in 12 and 24 wk old BKS-db/db mice and their non-diabetic db+ littermates (Fig. 2). We counted the numbers of Mt in the axons of myelinated and unmyelinated fibers in both dorsal and ventral roots. We also measured the areas of all fibers to confirm that changes in Mt number per axon were not an artifact from changes in fiber area. The areas of fibers were similar between db+ and db/db mice, so changes in Mt numbers per fiber represent a change in Mt density. The Mt density was unchanged between db+ and db/db axons at 12 wk of age and was also unchanged in unmyelinated fibers or in any ventral root fibers at 24 wk of age (not shown). There was a striking increase in the number of Mt in dorsal root fibers in db/db mice compared to db+ mice at 24 wk of age. The size of the Mt was unchanged, but notably, the Mt appeared swollen with distended cristae (Fig. 2). The data suggest that Mt biogenesis and/or fission was increased in the axons involved in the progression of diabetic neuropathy and that Mt function was impaired.

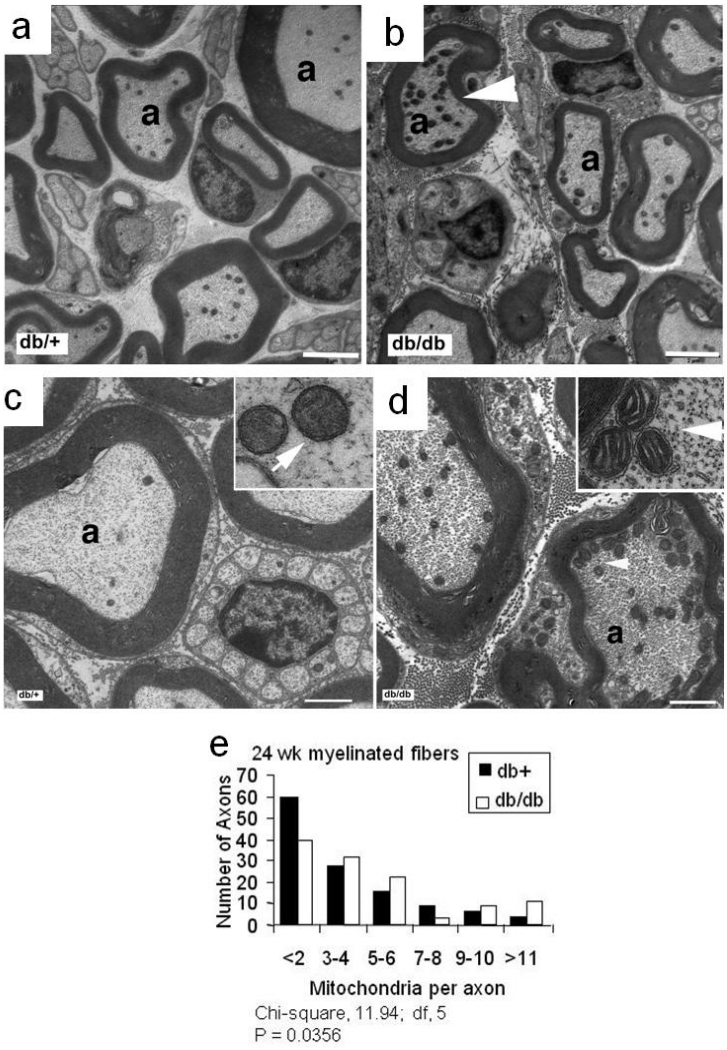

Figure 2. Mt Density and Morphology in Dorsal Root Axons of Diabetic Mice. Nerve roots were prepared for ultrathin cross sections for TEM. In dorsal roots at 24 wk, there was an accumulation of Mt in db/db mice (b, arrowhead). High magnification images of axons from dorsal roots of db+ animals (c) show normal Mt number while axons from dorsal roots of db/db animals (d) show increased numbers of Mt in axons (arrowhead) and increased neurofilaments and microtubules. In (c) and (d), each inset contains a higher magnification of the Mt (c; normal Mt) and (d; Mt with slightly dilated cristae). Scale bars = 2 μm in (a-b), 1 μm in (c-d). Quantitative analysis of Mt density in myelinated axons from dorsal roots is presented in the distribution plot (e). There were increased numbers of Mt in the dorsal root myelinated fibers of the diabetic (db/db) compared to control (db+) mice at 24 wk ($P<0.05$). There were no statistical differences in Mt density in dorsal root myelinated fibers between dbdb and db+ animals 12 wk of age (not shown).

To explore the mechanisms of increased Mt in the axons of diabetic mice, we returned to the cell culture model of exposure to hyperglycemia. Using a novel technique for the assessment of Mt DNA synthesis that was adapted in our laboratory [2], we assessed Mt biogenesis in the neurites. The development of this technique was a multistep process of adaptation and validation that is described in the next section of this report (Fig. 5-8). Using a co-labeling technique, we found that, similar to our previous work [6], there is a rapid (3-6 h) increase in the number of Mt in the neurites in high glucose. We now find that 20-25% of the Mt in the neurites are incorporating new DNA, suggesting that these are undergoing biogenesis in order to generate new Mt. Because 75-80% of the neurite Mt are not making new DNA, the data also suggest that Mt are accumulating in the neurites via fission and/or by altered transport.

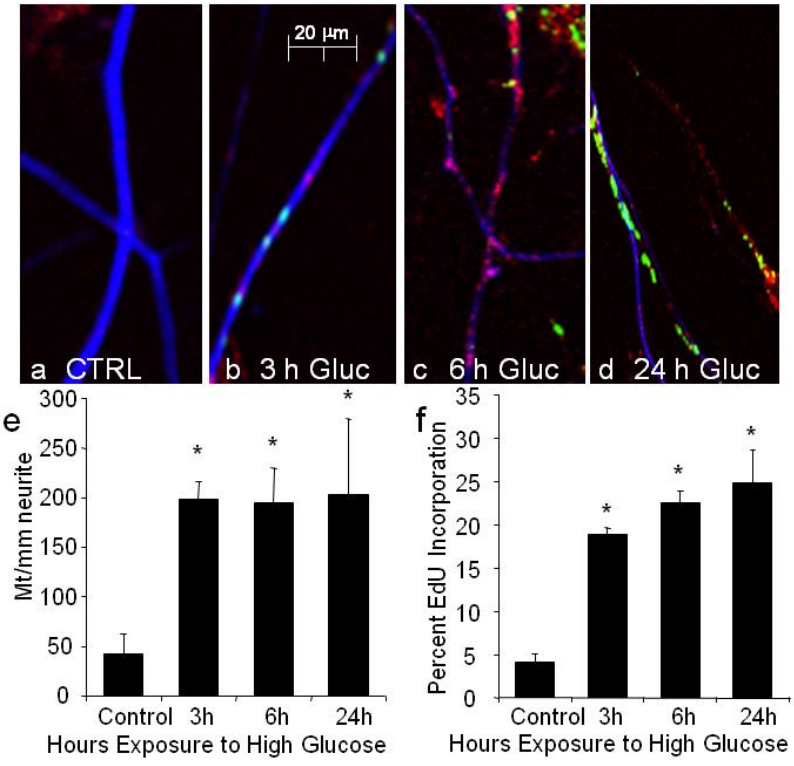

Figure 3. Hyperglycemia Increases Mt DNA Synthesis in Cultured DRG Neurons. DRG neurons from C57/Bl6 mice were exposed to 25.7 mM glucose for 0, 3, 6, or 24 h in the presence of EdU, then fixed and stained for EdU incorporation (green), Mt (PDH, red), and neurons (neurofilament, blue). (a) No Mt or EdU labeling was observed in neurites under control conditions. (b) EdU incorporation increased in neurites. In (c-d), both Mt labeling and EdU incorporation continued to increase in neurites with prolonged hyperglycemia. The high magnification images of neurites permit counting of the numbers of discrete Mt and the proportion of these incorporating EdU. Quantification of a-d is shown in (e-f). 2 separate experiments, each with 3 replicates and 3 images per condition, giving n=18 images were analyzed. The number of yellow (PDH and EdU positive) and red (PDH only) Mt in neurites were counted. The number of Mt was divided by the neurite length to give a measure of Mt/mm and the percent yellow Mt was calculated. *Mean number of Mt/mm and the percent incorporating EdU both increased significantly by 3 h compared to control glucose and remained elevated up to 24 h, $p<0.01$.

In order to determine whether fission is a prominent mechanism in hyperglycemia-induced increases in axonal Mt, we examined the expression and localization of the essential fission protein Drp1. Cultured adult mouse DRG neurons were exposed to control (5.7 mM) or high (25.7 mM) glucose for 6 or 24 h, then fixed and dual IHC labeled for the Mt protein VDAC and the fission protein Drp1 (Fig. 4). Both proteins are evident in the neurites under control conditions but they do not overlay. With increasing periods of exposure to high glucose, the level of VDAC increases in the neurites. Furthermore, VDAC begins to overlay with Drp1. At 6 h, short segments of the neurites show co-localization, notably closer to the growth cones. At 24 h, most of the neurite length contains co-localization of the labels, suggesting that there is a very high level of Mt fission occurring. We can conclude from these studies that Mt undergo biogenesis in high glucose. Increased Mt would disperse the load of excess metabolic

substrates. Furthermore, we know that Mt are rapidly oxidatively damaged in hyperglycemia [7-9], suggesting that biogenesis is also required to restore Mt function. However, Mt in neurites also undergo rapid and extensive fission. We contend that excessive Mt fission in hyperglycemia ahead of complete Mt biogenesis leads to Mt damage and neuronal cell injury, contributing to the progression of diabetic neuropathy.

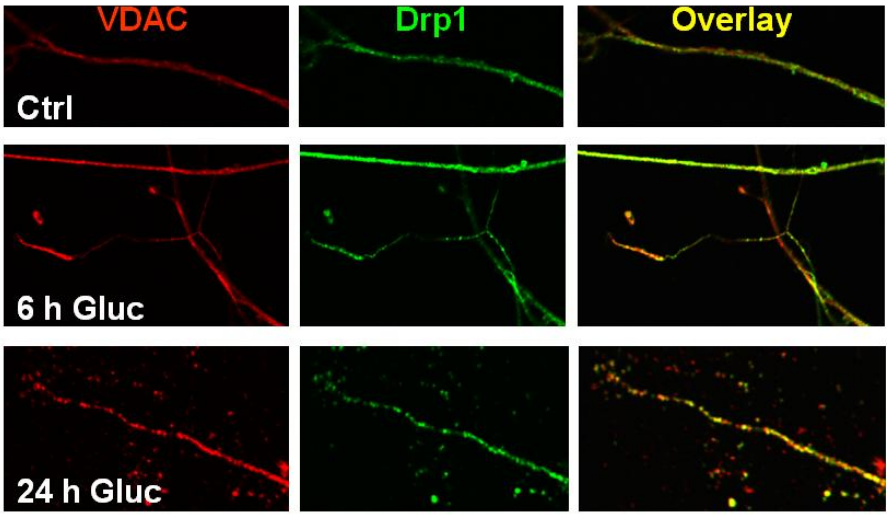

Figure 4. Hyperglycemia Promotes Mt Fission in the Neurites of DRG Neurons. DRG neurons from C57/Bl6 mice were exposed to 25.7 mM glucose for 0, 6, or 24 h, then fixed and immunolabeled for Drp1 (green) and Mt (VDAC, red). Co-localization of the labels, which demonstrates re-localization of Drp1 to Mt, suggesting Mt fission, appears in yellow and increases with time of exposure to high glucose.

Visualization of MtDNA Biogenesis

The regulation of Mt morphology and number within healthy cells by a dynamic balance of fission and fusion events appears essential to maintenance of neuronal cell function. Modulation of the fission/fusion balance is important in: (1) creating new Mt for dividing cells; (2) efficient dissemination of energy across cell structure (metabolic fission); and (3) apoptosis (apoptotic fission). In the nervous system the high energy demand of neurons makes these mechanisms particularly critical. Mt are distributed in all neuronal compartments, including the cell body, axons, dendrites, and synaptic terminals. Mt biogenesis allows neurons to meet changing energy loads and to redistribute Mt throughout all compartments of the neuron. As mentioned in the previous section, we developed a sensitive technique to label newly synthesized Mt DNA (MtDNA) in individual neurons by combining the incorporation of thymidine analogs into MtDNA with a tyramide signal amplification (TSA) protocol. This technique is a valuable tool for visualizing and measuring MtDNA biogenesis within individual neurons, and importantly, in specific compartments such as somas, dendrites, axons, and synapses.

We used the thymidine analogs BrdU and EdU to visualize newly synthesized MtDNA. The combination of either BrdU immunohistochemistry or EdU click chemistry with a TSA protocol significantly enhanced the visualization of BrdU and EdU incorporation into MtDNA. The specificity of the signals was verified with specific inhibitors of DNA polymerase α (nuclear) or DNA polymerase γ (Mt). Amplified BrdU and EdU signals were present in both nuclear DNA and MtDNA when F11 cells were incubated with for 12 hr (BrdU Figures 5A and 5C, EdU Figures 6A). F11 cells treated with aphidicolin, an inhibitor of DNA polymerase α, resulted in incorporation into MtDNA but not into nuclear DNA (BrdU Figure 5B, EdU Figure 6B).

Incorporation of BrdU/EdU into MtDNA was blocked by treatment of F11 cells with ethidium bromide or 2′,3′-dideoxycytidine, inhibitors of DNA polymerase γ, during the 12-hr incubation, whereas nuclear DNA synthesis was preserved (BrdU Figure 5D, EdU Figures 6C-D).

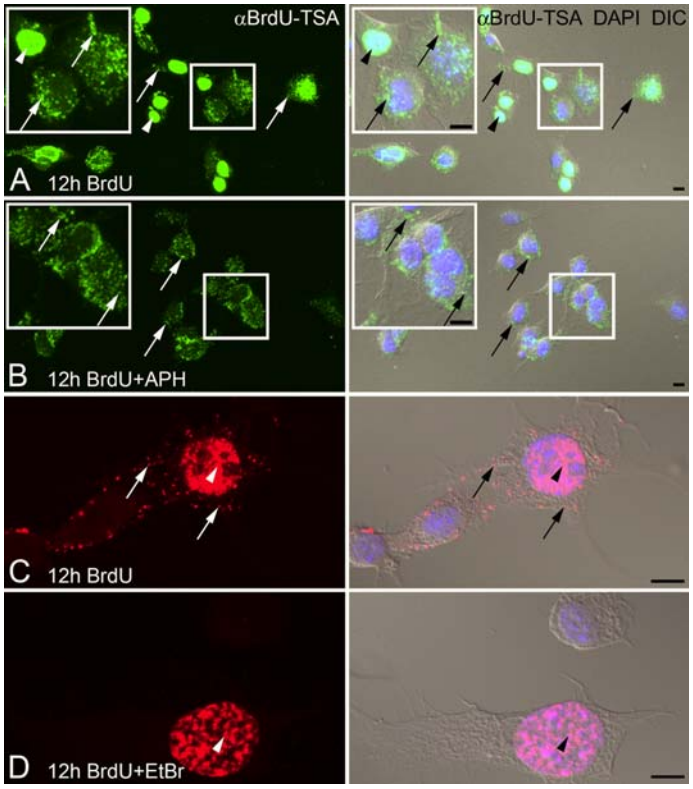

Figure 5. Inhibitors of nuclear (α) or Mt (γ) DNA polymerases differentially block BrdU incorporation. F11 neuroblastoma cells are incubated with BrdU for 12 hr with or without the addition of DNA polymerase inhibitors. Amplified BrdU signal [αBrdU-TSA, (A,B in green; C,D in red)] is compared with DNA stain (DAPI, blue) and cell morphology (DIC). (A,C) Cells incubated with BrdU show both nuclear DNA (arrowheads) and MtDNA (arrows) incorporation. Insets (A,B) show magnified views of the boxed areas to illustrate the detail of the BrdU signals. (B) Addition of 7 μM aphidicolin (+APH) inhibits nuclear incorporation of BrdU, whereas MtDNA labeling (arrows) is maintained. (D) Addition of 1.0 μg/ml of ethidium bromide (+EtBr) inhibits incorporation of BrdU into MtDNA but not into nuclear DNA (arrowhead). Bar = 10 μm.

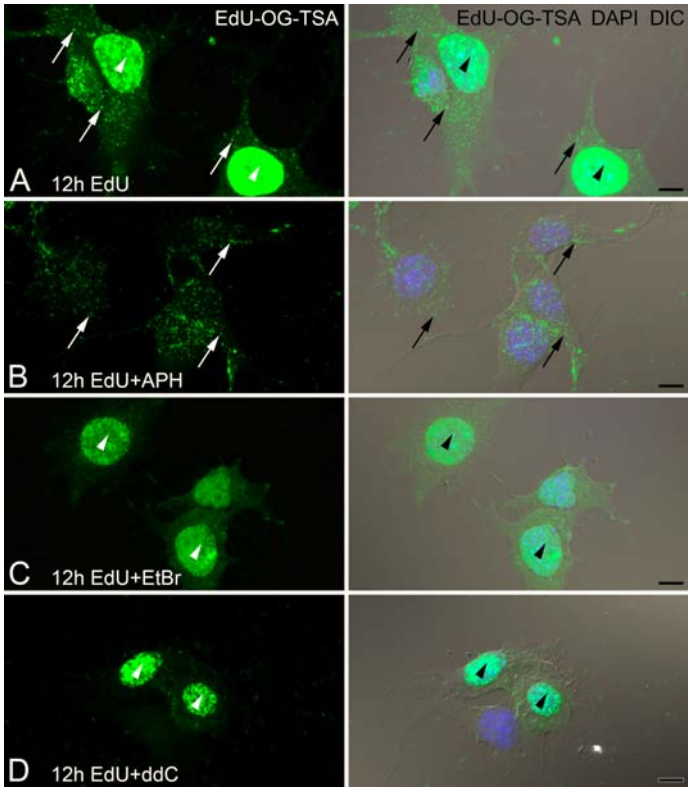

Figure 6. Inhibitors of nuclear (α) or Mt (γ) DNA polymerases differentially block EdU incorporation. F11 neuroblastoma cells are incubated with or without DNA polymerase inhibitors 4 hr prior to and together with EdU for an additional 12 hr. Amplified EdU signal (EdU-OG-TSA) is compared with DNA stain (DAPI, blue) and cell morphology (DIC). (A) Cells incubated with EdU show both nuclear (arrowheads) and MtDNA (arrows) incorporation. (B) Addition of 7 μM aphidicolin (+APH) inhibits nuclear incorporation of EdU, whereas MtDNA labeling (arrows) is maintained. (C) The presence of 1.0 μg/ml ethidium bromide (+EtBr) inhibits incorporation of EdU into MtDNA but not into nuclear DNA (arrowheads). (D) 2′,3′-Dideoxycytidine (+ddC, 200 mM) also inhibits MtDNA but not nuclear incorporation of EdU (arrowheads). Bar = 10 μm.

Cultured DRG neurons were also used to evaluate the utility of the TSA BrdU/EdU signals for newly synthesized MtDNA. Embryonic DRG neurons incubated with BrdU/EdU for 24 hr and processed with BrdU-TSA revealed a significant amount of MtDNA synthesis (BrdU Figures 7B and 7C, EdU Figure 8B). Most of the labeled MtDNA copies were located within the soma (BrdU Figures 7B and 7C, EdU Figures 8B-D). In some cases, positively labeled MtDNA was observed within the neurites (Figure 7D).

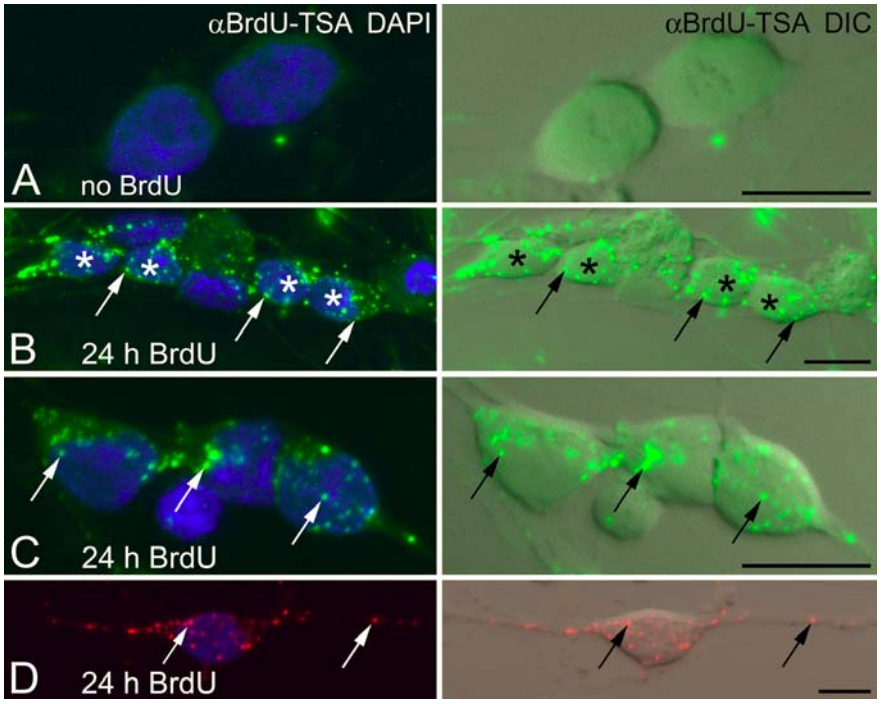

Figure 7. BrdU incorporation into MtDNA of primary sensory neurons. Embryonic dorsal root ganglion (DRG) neurons are incubated with BrdU for 24 hr. Amplified BrdU signal (αBrdU-TSA; B and C in green, D in red) is compared with DNA stain (DAPI, blue) and cell morphology (DIC). (A) In the absence of BrdU, no false labeling is present after TSA immunofluorescence. (B,C) BrdU is clearly incorporated into MtDNA (arrows) of DRG neurons. Asterisks in B identify DRG nuclei. (D) BrdU incorporation into MtDNA (arrows) is present in the soma and neurites of DRG neurons. Bar = 10 μm.

The EdU protocol allowed for subsequent fluorescent labeling of other cellular structures or proteins by eliminating the harsh HCl DNA denaturation step that is necessary for exposing the BrdU epitope. SH-SY5Y cells grown in the presence of EdU for 6 hr colocalized with a Mt protein, PDH, further supporting the specificity of the MtDNA signal (Figure 8A). There was no difference in the quality (Figures 7B–D and 8B) or quantity (Figure 8E) of positively labeled MtDNA in embryonic DRG neurons after 24-hr exposure to either BrdU or EdU. Cultured DRG neurons from adult mice also demonstrated EdU labeling of MtDNA (Figures 8C and 8D). Adult DRG neurons were identified with a pan-neuronal marker (Tuj1) or a subtype-specific marker (trkA receptor). The number of EdU-labeled MtDNA copies was more abundant in trkA-labeled adult neurons, compared with NGF-dependent embryonic DRG neurons after 24 hr in vitro (Figure 8E). Adult neurons are consistently larger than embryonic DRG neurons, and when the number of labeled MtDNAs per neuron was corrected for cell volume, the embryonic neurons were more actively replicating MtDNA than were adult neurons (Figure 8F).

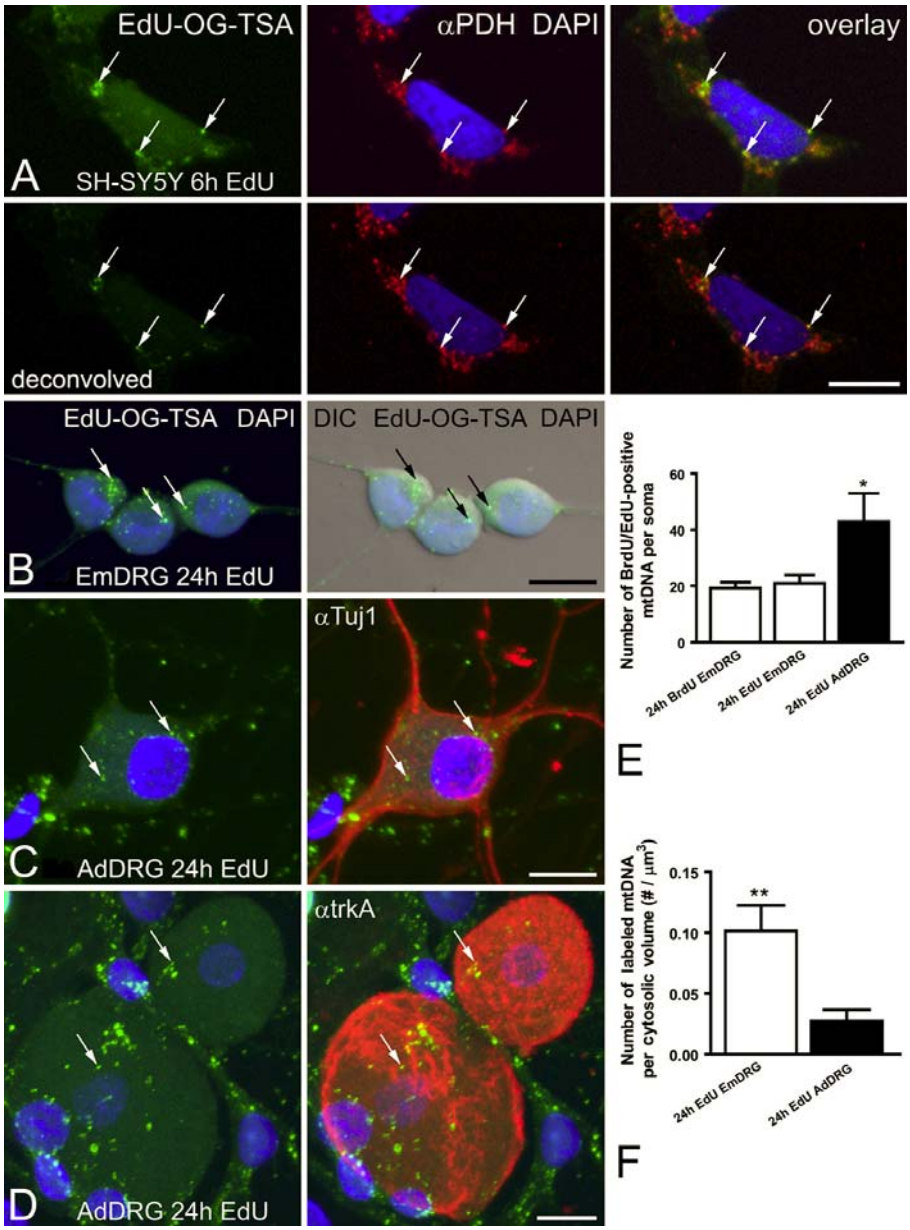

Figure 8. Amplified EdU signal in MtDNA is associated with Mt and other cell-specific markers. (A) SH-SY5Y neuroblastoma cells are incubated with EdU for 6 hr. Amplified EdU signal (EdU-OG-TSA, green) is compared with DNA stain (DAPI, blue) and a Mt marker, pyruvate dehydrogenase (αPDH, red). EdU signal (arrows) localizes to Mt. Lower panels in A are deconvolved signals and demonstrate a clear association of MtDNA within Mt. (B,C) Embryonic or adult DRG neurons are incubated with EdU for 24 hr. EdU signal (EdU-OG-TSA, green) is compared with DNA stain (DAPI, blue) and cell morphology (in B, DIC). (B) EdU signal is present in MtDNA (arrows) of embryonic DRG neurons (EmDRG). (C,D) EdU incorporation into MtDNA (arrows) is present in adult DRG neurons (AdDRG), identified by a pan-neuronal marker (C, αTuj1, red) or a subtype-specific marker (D, αtrkA, red). (E) The number of EdU-positive MtDNAs per embryonic DRG soma is comparable to the number of BrdU-positive MtDNAs after 24-hr incubation (white bars). Adult DRG neurons have significantly more EdU-positive MtDNAs (black bar) compared with embryonic DRG neurons. Error bars indicate mean ± SEM for 20 DRG somas per group, *p,0.05. (F) MtDNA replication is more active in embryonic than in adult DRG neurons. Error bars indicate the mean ± SEM number of EdU-positive MtDNAs corrected for cytosolic volume (soma volume – nucleus volume). Embryonic DRG somas (white bar, n=20) have significantly more MtDNA replications per cytosolic volume compared with adult DRGs (black bar, n=20), **p,0.01. Bar = 10 μm.

Mt dynamics and biogenesis are regulated by a variety of cellular mechanisms and have a significant impact on health and disease. We developed a sensitive assay to visualize and quantify newly synthesized MtDNA in individual cells. The utility of this signal amplification technique to visualize and measure newly synthesized MtDNA with EdU and BrdU at the cellular level will considerably advance experiments in our laboratory that examine the regulation of Mt biogenesis in the context of diabetes and diabetic neuropathy.

The effects of anesthesia on measures of nerve conduction velocity

Nerve conduction velocity (NCV) is a reproducible measure of peripheral nerve function used to assess and diagnose DPN. Multiple factors affect NCV beyond the disease condition being studied including ambient temperature, needle placement, the intensity of the electrical stimulus and the degree and type of anesthesia. NCV in humans is performed while the patient is awake and responsive. This is usually not the case for animal experiments. By definition, anesthesia slows or blocks nerve impulses and affects synaptic transmission and neuronal function [10-12]. We examined four commonly used anesthesia methods including isoflurane (ISO), pentobarbital (PB), ketamine/xylazine (KX) and 2,2,2-tribromoethanol (TBE) and documented their effects on NCV in the C57Bl6/J mouse.

Anesthesia and Physiological Parameters

Male C57BL/6 mice (n=40) were purchased from The Jackson Laboratory (Bar harbor, ME) at 12 weeks of age. Mice were randomly assigned to one of four groups receiving the following anesthesia, isoflurane (ISO), ketamine/xylazine (KX), pentobarbital sodium (NB) and 2-2-2 tribromoethanol (TBE), n=10 per group. The experimental protocol and dosages are presented in Table 1. Onset of anesthesia was judged by diminish righting reflex and decreased pedal withdrawal. Physiological parameters were recorded during the first 5 min of anesthesia. The ambient room temperature was maintained at 22° C. Monitoring included skin temperature (ear, proximolateral hind limb, tail and dorsal foot) by infrared thermometer (Fluke 63, Everett, WA), core body temperature (Cole-Parmer Instrument Company, Vernon Hills, IL), and cardiopulmonary variables (oxygen saturation, heart rate, and respiratory rate) using a pulse oximeter (Mouse Ox; Starr Life Sciences Corp, Oakmont, PA).

Table 1

Group (n=10)	Drug Dosage (12wk, 24wk)	Source
Isoflurane (ISO)	4-5% for induction 1-2% for maintenance	Hospira, Inc., Lake Forest, IL
Ketamine/Xylazine (KX)	Ketamine 100mg/kg Xylazine 5mg/kg	Fort Dodge Animal Health, Fort Dodge, IA/Ben Venue Laboratories; Bedford, OH
Pentobarbital (PB)	50mg/kg	Ovation Pharmaceutical Inc., Deerfield, IL
2-2-2 tribromoethanol (TBE)	200mg/kg	Sigma-Aldrich, St. Louis, MO

All drugs were administrated by intraperitoneal injection with the exception of isoflurane.

Nerve Conduction Studies

Motor and sensory NCV were measured in the tail and hind limb. The expected increase in both motor and sensory NCV with age was noted in the hind limb and tail and was not affected by anesthesia. Sensory NCV measured in the hind limb and tail was not differentially affected by any of the anesthetics (Table 2). A significant decrease in SMNCV was detected in the KX and TBE groups at 12 weeks and the PB, KX and TBE groups at 24 weeks

of age compared to ISO (Table 2). Additionally, there was a significant increase in latency in the TDML at 12 weeks in the TBE group compared to the ISO group (Table 2).

Table 2. NCV following anesthesia

Age	12 weeks ISO	PB	KX	TBE	24 weeks ISO	PB	KX	TBE
SNCV (m/sec)	24.80±.55 n=10	23.70±1.22 n=10	23.56±.78 n=9	22.50±.64 n=10	27.63±.50 n=8	26.67±.69 n=9	26.75±.53 n=8	26.83±.83 n=6
SMNCV (m/sec)	56.33±2.5 n=9	51.7±2.9 n=10	44.70±1.3* n=10	43.10±1.1* n=10	62.88±2.0 n=8	49.56±1.5* n=9	52.38±1.2* n=8	49.67±2.1* n=6
TSNCV (m/sec)	32.11±.45 n=9	30.60±.4 n=10	32.56±.41 n=9	31.20±.66 n=10	33.00±78 n=6	30.57±.1.54 n=7	31.86±94 n=7	30.00±.32 n=5
TDML sec	1.71±.03 n=10	1.89±.04 n=9	1.88±.03 n=9	1.94±.03* n=10	1.76±.09 n=7	1.91±.03 n=9	1.81±.08 n=8	2.0±.06 n=5

Motor and sensory NCV were measured in the sural, sciatic-tibial and caudal tail nerves. The type of anesthesia did not result in significant differences in SNCV or TSNCV. ± SEM, ISO = Isoflurane, PB = Pentobarbital, KX = Ketamine/Xylazine, TBE = 2-2-2 tribromoethanol. * $p < 0.05$ compared to ISO.

Surface and Core Temperature

Peripheral nerves lie close to the surface; therefore, we assessed the effects of anesthesia on surface temperature. When compared to ISO, mice anesthetized with KX exhibited a significantly lower surface temperature measured at the ear, dorsal foot and hind limb at 12 weeks of age (Table 3). This effect was also observed in the hind limb at 24 weeks of age (Table 3). At 24 weeks of age, PB, KX and TBE treated animals exhibited significantly decreased surface temperature measured at the hind limb (Table 3). Core temperature measured in mice at 24 weeks of age demonstrated similar effects of anesthesia as surface measures with significant decreases in animals treated with PB, KX and TBE (Table 3).

Table 3. Surface and Core Temperature

Age	12 weeks				24 weeks			
	ISO	PB	KX	TBE	ISO	NB	KX	TBE
Ear	29.03±.37 n = 8	28.04±.71 n = 10	26.90±.40* n = 10	27.80±.24 n=10	29.80±.65 n=7	27.67±.13 n=9	27.60±.51 n=9	28.53±.26 n=6
Tail	23.65±.21 n = 8	22.78±.35 n = 10	23.6±.44 n = 10	23.36±.13 n=10	25.71±1.6 n=7	24.42±.1.2 n=9	23.9±.19 n=9	23.6±.27 n=6
Foot	24.23±.22 n = 8	22.3±.28* n = 10	22.9±.35* n = 10	23.9±.16 n=10	23.91±.15 n=7	23.04±.23 n=9	23.78±.34 n=9	23.37±.39 n=6
Hind Limb	24.95±.14 n = 8	23.2±.16* n = 10	23.22±.30* n = 10	24.08±.17 n=10	27.33±.39 n=7	24.5±.43* n=8	24.28±.32* n=8	24.08±.34* n=5
Core	NA	NA	NA	NA	34.96±.17 n=8	31.19±.32 n=9	29.57±.66 n=9	31.48±.27 n=6

The effect of anesthetic agents on surface temperature measured on the ear, dorsal hind paw, tail and lateral hind limb and rectal core temperature. For each drug temperatures were monitored at 12 week and 24 weeks of age. ± SEM, ISO = Isoflurane, PB = Pentobarbital, KX = Ketamine/Xylazine, TBE = 2-2-2 tribromoethanol. * $p < 0.05$ compared to ISO.

Cardiopulmonary Function

Anesthesia depresses heart function and blood flow [13] which may affect both surface temperature and potentially blood flow to the peripheral nervous system. We assessed the effects of ISO, PB, KX and TBE on heart rate, arterial oxygen saturation and respiratory rate. Compared to ISO anesthesia (451.1±7.109), heart rate (HR) was significantly reduced by PB (321.7±16.28), KX (197.2±13.46) and TBE (381.7±8.125) (Fig 9a). Oxygen saturation was also

significantly decreased by PB (90.85±1.8) and TBE (88.97±3.5) compared to ISO (99.36±.04) (Fig. 9b). The method of anesthesia also had an impact on respiratory rate. Compared to ISO, KX anesthesia significantly decreased respiratory rate (Fig. 9c).

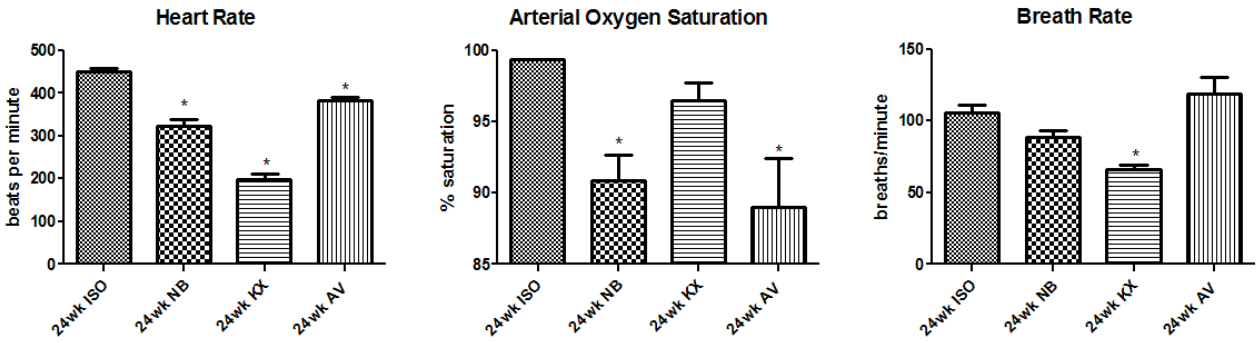

Figure 9. The effects of anesthesia on cardiopulmonary function (heart rate, arterial oxygen saturation and respiratory rate). All parameters were measured under anesthesia in mice 24 weeks of age and within 5 min of anesthesia. * = $p < 0.05$

Liver Function and Mortality

When performed carefully, NCV may be measured at multiple time points throughout the developmental time course of a disease. Therefore, any long term toxicity may affect both the disease under study and independently affect NCV. We assessed liver toxicity following the two (12 wk and 24 wk) doses of anesthesia. Serum activities of aspartate transaminase (AST) and alanine transaminase (ALT) were measured (data not shown) to determine the effect of anesthetic agents on liver function. All four agents, at the recommended dosage, did not cause significant changes and were within the reference levels [14]. Increased animal mortality was observed following treatment with TBE [15-16]. Five of these animals developed peritonitis and died [15-16]. Five other mice, two from the ISO group, one from the PB group and two from the KX group died while anesthetized.

We compared the effects of ISO, KX, PB and TBE on motor and sensory NCV. We also documented their effects on surface and core temperature, heart and respiratory rates and oxygen saturation and performed simple tests of liver function. We determined that motor NCV was decreased following anesthesia induced by KX and TBE compared to ISO, while sensory NCV was consistent. Surface temperature in the hind limb, heart rate and oxygen saturation were also affected by the different modes of anesthesia.

Due to the increase in circulating blood glucose, decreased oxygen saturation and increased mortality following TBE administration, we would discourage its use for any rodent study. KX anesthesia is safe, effective and relatively easy to administer for procedures of longer duration, e.g. survival surgery; however, its effects on blood glucose should be considered in models of diabetic complications. PB is similar to KX with no effect on blood glucose but significantly decreases oxygen saturation. All of the injectable anesthetics require time to take effect and often require supplemental dosing leading to accidental overdose. ISO anesthesia is fast, easily monitored, has the least impact on NCV, surface and core temperatures and cardiopulmonary function and the least toxic effects. We highly recommend its use for short term procedures such as measures of NCV in all models of peripheral nerve disease.

Mechanical allodynia in painful diabetic neuropathy

Painful Diabetic Neuropathy (PDN) affects more than 25% of patients with type 2 diabetes; however, the pathogenesis remains unclear due to lack of knowledge of the molecular mechanisms leading to PDN. We are currently using an animal model of type 2 diabetes in order to understand the roles of p38 in PDN. The C57BLK db/db (db/db) mouse carrying a loss-of-function mutation in the leptin receptor, is hyperphagic, obese, and develops type 2 diabetes. These mice develop mechanical allodynia in the hind paws during the early stage (6-12 wk of age) of diabetes [17]. Thus, we can use this timeline of PDN in the db/db mouse to explore the signaling mechanisms underlying mechanical allodynia.

p38 is phosphorylated during the time period of mechanical allodynia

We previously characterized the time-course of mechanical allodynia in db/db mice from 6-12 wk of age. The maximum reduction of mechanical pain thresholds was detected at 8 wk of age [17]. In the current study, pp38 immunoblots were performed on lumbar DRG (LDRG) collected at 5, 8, 10, and 12 wk of age (Fig. 10). Representative pp38 immunoblots demonstrate increased phosphorylation of p38 in LDRG of the db/db mice in comparison to the db+ nondiabetic littermates at 5, 8 and 10 wk of age. At 12 wk of age, p38 phosphorylation in db/db mice was reduced to the control level (Fig. 10A & B).

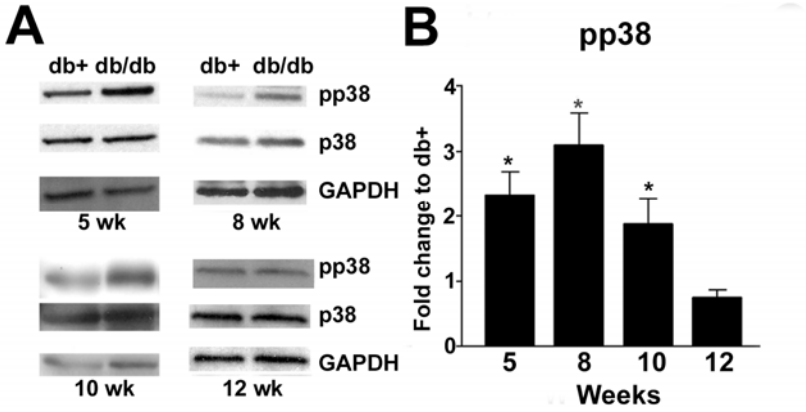

Figure 10. Phosphorylation of p38 during the course of mechanical allodynia. A: Representative immunoblots of pp38, p38 and GAPDH using LDRG extracts from db+ and db/db mice at 5, 8, 10, and 12 wk of age. In addition, no change in expression levels of p38 was detected in LDRG of db/db mice and db+ mice. GAPDH served as the loading control. B: Densitometric analysis of immunoblots using LDRG of db+ and db/db mice at 5, 8, 10 and 12 wk of age during the development of mechanical allodynia. n = 4, *$p < 0.05$.

We next localized pp38 in L4-6 DRG using immunohistochemistry (Fig. 11). pp38 immunoreactivity was detected mostly in the nuclei of small- to medium-sized neurons in L4-6 DRG of db/db, but not db+, mice (Fig. 11B, arrow). The most prominent increase was detected at 8 wk of age, with a 6-fold increase in the percentage of pp38-positive neurons in db/db mice in comparison to db+ mice (Fig. 11C). A cell size distribution study detected significant increases of not only the percentages of pp38 positivity in small- (<20 μm in diameter) to medium-sized (20-40 μm in diameter) LDRG neurons, but also in large-sized (>40 μm in diameter) LDRG neurons in db/db mice at 8 wk of age (Fig. 11D).

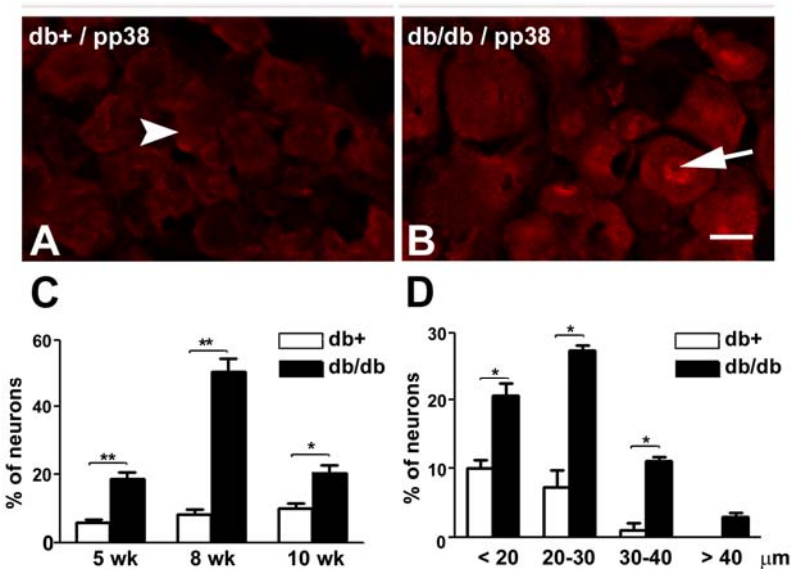

Figure 11. pp38 immunohistochemistry in LDRG of db+ and db/db mice. A, B: Representative images of pp38 immunohistochemistry in LDRG from db+ (A) and db/db (B) mice at 8 wk of age. Increased nuclear immunoreactivity was detected in db/db (arrow) but not db+ (arrowhead) LDRG neurons. Bar = 15 μm. C: Quantitation of pp38-positive LDRG neurons in db+ and db/db mice. n = 6, *p < 0.05, **p < 0.01. *p < 0.05, one-way ANOVA test. D: Cell size distribution of pp38-positive LDRG neurons at 8 wk of age. n = 4, *p < 0.05.

Anti-NGF inhibits the phosphorylation of p38 in db/db mice

Previously, we reported enhanced NGF expression and phosphorylation of Trk A receptors in LDRG of db/db mice during the period of mechanical allodynia. To investigate if NGF is an upstream activator of p38 during the period of mechanical allodynia in db/db mice, we administered the same anti-NGF antibody used in our previous studies to block the development of mechanical allodynia [17]. pp38 immunoblots were performed to determine the effects of anti-NGF on p38 phosphorylation in LDRG following 2 weeks of anti-NGF treatment, following the same paradigm as our previous studies [17]. Treatments with anti-NGF at 6 and 7 wk of age significantly decreased the phosphorylation of p38 in LDRG of db/db mice at 8 wk of age (Fig. 12A). Densitometric studies further determined that anti-NGF reversed the p38 phosphorylation in db/db mice but did not affect the baseline p38 phosphorylation in LDRG of db+ nondiabetic mice (Fig. 12B).

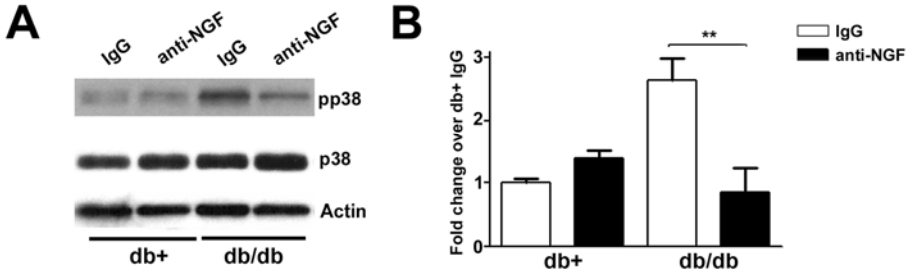

Figure 12. Anti-NGF treatment inhibits the phosphorylation of p38 in db/db mice. A: Representative immunoblots of pp38, p38 and actin using LDRG from db+ and db/db mice treated with either control (IgG) or an anti-NGF antibody for 2 wk. B: Densitometric studies of pp38 immunoblots using LDRG from 8 wk old db+ and db/db mice. n= 4, **p < 0.01.

Intrathecal administration of SB203580 inhibits p38 phosphorylation and mechanical allodynia

To determine directly if the activation of p38 mediates mechanical allodynia in db/db mice, a p38 inhibitor, SB203580, was administered intrathecally via mini osmotic pumps. Minipumps were inserted into both db+ and db/db mice at 7 wk of age and delivered SB203580 in artificial CSF with 10% DMSO at a rate of 0.51 μg/hr for 7 d. Control groups were treated with artificial CSF with 10% DMSO. Mechanical thresholds were measured at the end of the

SB203580 treatment. pp38 immunoblots confirmed the inhibition of p38 phosphorylation in LDRG in response to SB203580 treatment in both db+ and db/db mice (Fig. 13A). Densitometric analysis demonstrated a reversal of p38 phosphorylation in db/db mice down to the levels observed in the control db+ mice (Fig. 13B). In conjunction with the inhibition of p38 phosphorylation, SB203580 treatment inhibited mechanical allodynia in db/db mice (Fig. 13C) and lowered the percentage of substance P (SP)-positive neurons (Fig. 13D). In contrast, the percentage of Isolectin B-4 (IB4)-labeled neurons was not affected by SB203580 treatment (Fig. 13E).

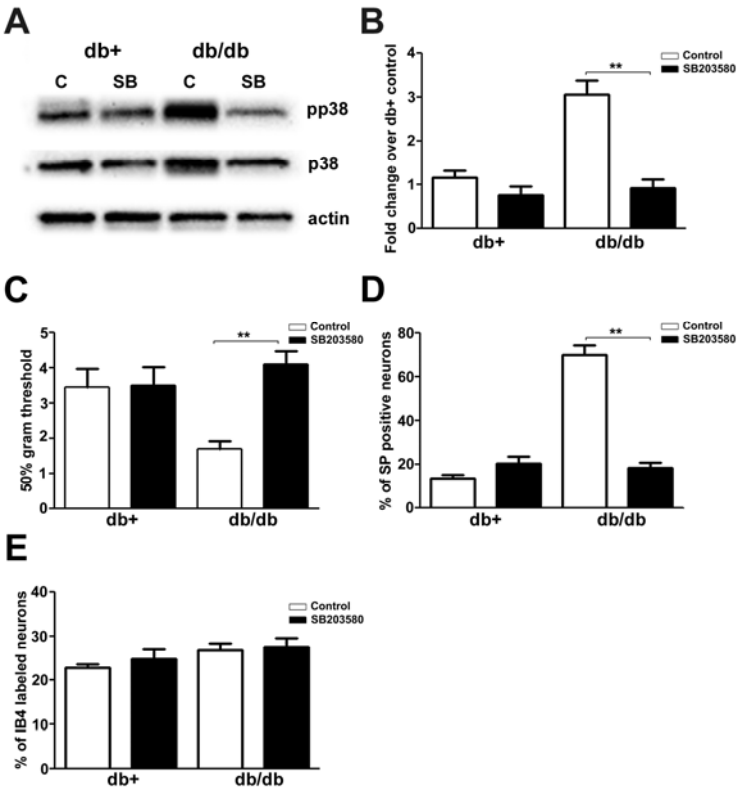

Figure 13. SB203580 inhibits p38 phosphorylation, mechanical allodynia, and the percentage of SP-positive LDRG neurons in db/db mice. A: Representative immunoblots of pp38, p38 and actin from db+ and db/db LDRG at 8 wk of age after 1 wk of intrathecal treatments of vehicle (control CSF with 10 % DMSO) (C) or vehicle with SB203580. B: Densitometric studies of pp38 immunoblots demonstrated significant inhibition of p38 phosphorylation in db/db mice. C: SB203580 treatment reversed the decrease in mechanical thresholds (allodynia) in db/db mice. D: SB203580 treatment also lowered the elevated percentages of SP-positive LDRG neurons in control db/db mice compared to control db+ mice. E: SB203580 treatment had no effect on the percentage of IB4-labelled LDRG neurons in db+ and db/db mice. n = 4, **p < 0.01.

Intrathecal administration of SB203580 inhibits the upregulation of inflammatory mediators in LDRG of db/db mice

To study the downstream molecules of NGF-p38 signaling, we screened several nociceptive molecules reported to be involved in p38-mediated pain, including COX2, iNOS, and TNF-α. Immunoblots of COX2, iNOS, and TNF-α (Fig. 14A) were performed in order to quantify the levels of these inflammatory proteins. Densitometric analysis confirmed that the levels of COX2 (Fig. 14B), iNOS (Fig. 14C) and TNF-α (Fig. 14D) were increased in db/db mice in comparison to levels detected in db+ mice. SB203580 treatment inhibited this upregulation of inflammatory protein expression. However, in contrast to what is observed in db/db mice, SB203580 treatment did not have an effect on the protein levels of db+ mice (Fig. 14).

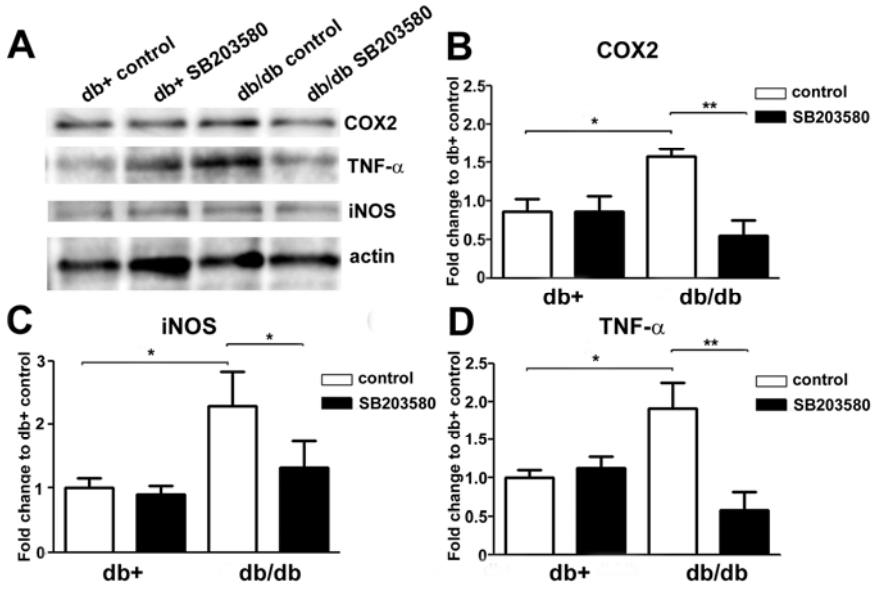

Figure 14. SB203580 treatment inhibits protein expression of inflammatory mediators in db/db mice. A: Representative immunoblots of LDRG from db+ and db/db mice. After 1 wk treatments with vehicle control or vehicle with SB203580, immunoblots were performed for iNOS, COX2, and TNF-α. Increased protein levels for all three inflammatory mediators were demonstrated in LDRG of db/db mice compared to db+ littermates. This upregulation was inhibited by treatment with SB203580. Actin served as a loading control. B, C, D: Densitometric analysis of COX2 (B), iNOS (C), and TNF-α (D) demonstrated significant upregulation of each respective protein in db/db mice that is inhibited by SB203580. N = 4, *p < 0.05, **p < 0.01.

P38 has been reported to mediate many types of pain [18]. Here we are the first to report a role for this protein kinase in mechanical allodynia associated with PDN in an animal model of type 2 diabetes. Previously, we reported that NGF-Trk A signaling is elevated in db/db mice [17]. The current study focuses on the mechanism underlying this role of p38 kinase in PDN and demonstrates that p38 is phosphorylated via NGF signaling in DRG neurons in the type 2 diabetic model. In turn, NGF-mediated p38 phosphorylation leads to mechanical allodynia in the db/db mouse by upregulation of multiple inflammatory mediators in LDRG.

The current study demonstrates the phosphorylation of p38 and the upregulation of multiple inflammatory mediators including COX2, iNOS, and TNF-α in DRG neurons of db/db mice. Our data suggest that inflammation in DRG could mediate mechanical allodynia in type 2 diabetes. While current guidelines for treating PDN only use neuropathic pain regimens [19], our results suggest that a combination of both neuropathic and anti-inflammatory therapies that target COX2, iNOS, and TNF-α will improve the current standard treatment for PDN of type 2 diabetes. Since p38 mediates multiple inflammatory mediators in PDN of type 2 diabetes, clinical studies using p38 inhibitors could potentially provide a better approach than using multiple inhibitors for mediators downstream of this mechanism to alleviate PDN of type 2 diabetes [20].

Insulin resistance in cortical neurons

A frequent complication related to diabetes is that diabetic patients experience increased functional disability following a stroke. We hypothesized that cortical neurons develop insulin resistance in diabetes and that this decreases circulating insulin and insulin-like growth factor-I (IGF-I)-mediated neuronal protection. We explored the effects of prolonged hyperinsulinemia leads on insulin signaling in cortical neurons. Decreased sensitivity to neuroprotective ligands may explain the increased neuronal damage reported in both experimental models of diabetes and diabetic patients following ischemia-reperfusion injury. This work was recently submitted to Antioxidants & Redox Signaling.

We began by examining the effects of hyperglycemia on neurons of the central nervous system. These studies arise because stroke is the 3rd leading cause of death behind heart disease and cancer. It is clear from epidemiological studies that diabetes exacerbates and/or is a principal cause of both stroke and heart attack. Ischemic stroke is a major macrovascular complication of diabetes and diabetic patients consistently exhibit poorer outcomes and prognoses than non-diabetic patients following a stroke.

Recent epidemiological studies suggest that the insulin resistance associated with type 2 diabetes is a risk factor for stroke [21-22]. Patients with diabetes show 2-6 fold increase in the risk of stroke compared to non-diabetic individuals. Furthermore, population-based cohort studies demonstrate that healthy individuals with metabolic syndrome also demonstrate a significant increase in stroke as well as cardiovascular mortality [23-24]. Insulin resistance increases the risk of stroke recurrence and, cumulatively, a poorer outcome and increased mortality after stroke [25-27]. While these studies clearly document the correlation of diabetes and stroke, the underlying mechanism has yet to be identified. Multiple factors including hyperglycemic neuronal injury and neuronal insulin resistance may contribute to increased ischemia-reperfusion-induced neuronal damage.

As a first step we measured insulin and IGF-I signaling in cultured primary cortical neurons. Immunohistochemistry for Tau5 (a neuron specific marker) confirmed neuronal phenotype (Fig 15A). From day 3 to day 6 *in vitro*, cortical neurons extended neurites and appeared more mature (Fig 15A). Both insulin and IGF-I influence the development of cortical and hippocampal neurons by promoting neurogenesis, survival, and differentiation [28-31]. To examine insulin and IGF-I signaling in our system, cortical neurons were treated with 20 nM insulin or IGF-I for 0 – 2 h followed by western immunoblotting. Insulin stimulation induced a time-dependent increase in the phosphorylation (i.e. activation) of intracellular signaling molecules including insulin receptor (InsR), Akt, glycogen synthase kinase 3β (GSK3β), and p70S6K (Fig 15B). Phosphorylation of ERK was not prominent and in many cases, not different from the control (untreated neurons). IGF-I treatment also resulted in a similar response as insulin.

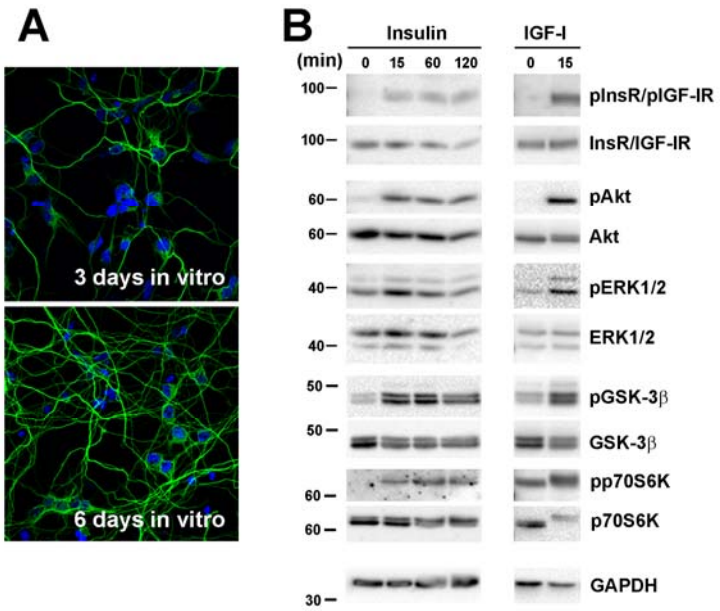

Figure 15. Insulin and IGF-I signaling in cultured cortical neurons. (**A**) Cortical neurons were harvested from E15 rat embryos. The cells were cultured for 3 or 6 days and immunolabeled for tau, a neuron-specific microtubule associated protein (green, detected by tau5 Ab). Nuclei were visualized with DAPI (blue). (**B**) Cortical neurons cultured for 7 days were stimulated with 20 nM insulin or IGF-I for 0-2h. Cell lysates were prepared in RIPA buffer and immunoblotted with the indicated antibodies. These experiments were repeated at least 3 times and a representative result is shown.

Hyperglycemia, dyslipidemia and hyperinsulinemia are characteristic of type 2 diabetes and the metabolic syndrome; all of which may contribute to insulin resistance [24, 32-33]. We next examined the contribution of each of these factors to insulin resistance in cortical neurons. To create an *in vitro* model of the metabolic syndrome in order to assess insulin

resistance, cortical neurons were treated with 25 mM added glucose, 0.2 mM palmitic acid (PA), or 20 nM insulin for 24 h. The media was then replaced with fresh treatment media and the cells exposed to 20 nM insulin for 15 min. In untreated cortical neurons, Akt is activated following 15 min of insulin treatment. 24 h insulin treatment reduced the response to subsequent short term insulin treatment. In contrast, 24 h glucose or PA exposure had no effect on the activation of Akt in response to short term insulin treatment (Fig 16A). Full activation of Akt requires sequential phosphorylation of Thr308 and Ser 473 by PDK1 and mTORC2, respectively [34]. 24 h insulin treatment decreased the phosphorylation of both of these sites as well as the increase in basal phosphorylation (Fig 16B). In parallel with the effect on Akt phosphorylation, 24 h insulin treatment also reduced short term insulin-stimulated p70S6K and GSK3β phosphorylation (i.e. activation of p70S6K and inactivation of GSK3β). Total protein levels of p70S6K and GSK3β were not affected. 24 h insulin treatment reduced IGF-I-stimulated Akt phosphorylation (Fig 16C).

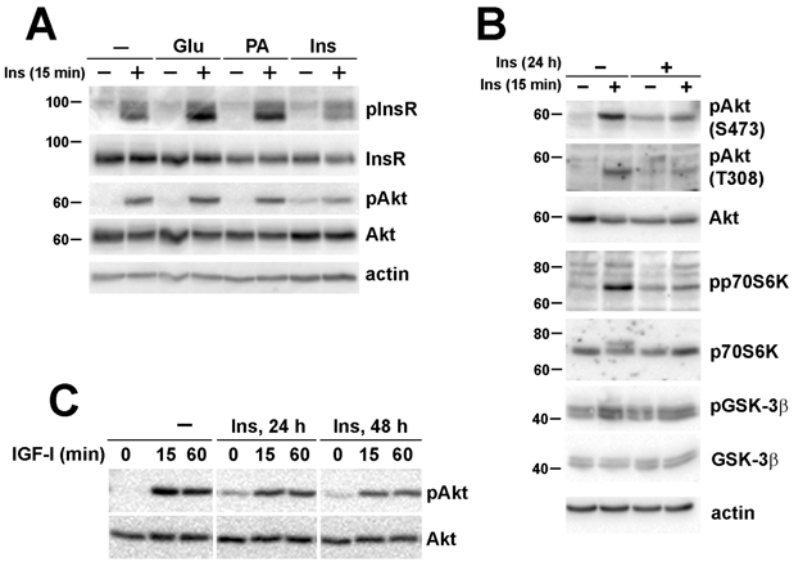

Figure 16. Chronic insulin treatment reduces insulin stimulated phosphorylation of Akt and downstream signaling molecules. (**A**) Cortical neurons were incubated with 25 mM glucose (Glu), 0.2 mM palmitic acid (PA) or 20 nM insulin (Ins) for 24 h and then stimulated with 20 nM insulin for 15 min. (**B**) The cells were treated without or with 20 nM insulin for 24 h and then stimulated with 20 nM insulin for 15 min. (**C**) The cells were pretreated with insulin for 24 or 48 h and then stimulated with 20 nM IGF-I for 0, 15, or 60 min. Cell lysates were prepared in RIPA buffer and immunoblotted with the indicated antibodies. These experiments were repeated at least 3 times and a representative result is shown.

We next explored the possible mechanism behind the reduction in Akt activation following chronic insulin-treatment. During 24 h insulin treatment, cortical neuron cultures were incubated without or with inhibitors of Akt (LY294002) or MAPK (U0126) signaling pathways. Following 24 h the cells were washed with HBSS and incubated in fresh treatment media (without insulin or inhibitors) for 30 min. The cultures were then treated with 20 nM insulin for 15 min. As in the previous experiments, cortical neurons chronically pretreated with insulin followed by acute insulin treatment exhibited reduced Akt phosphorylation (Fig 17). Combined treatment with insulin and the PI 3-K inhibitor, LY294002, restored Akt phosphorylation by acute insulin to control levels. The MAPK inhibitor U0126 had no affect on Akt phosphorylation. As in the previous experiments, ERK phosphorylation was not significantly affected by 24 h insulin treatment or by either inhibitor. The phosphorylation pattern of p70S6K and GSK3β paralleled that of Akt phosphorylation confirming the upstream requirement of Akt for the activation of these signaling molecules. These results suggest that chronic hyperactivation of Akt by insulin prevents further activation by acute insulin treatment.

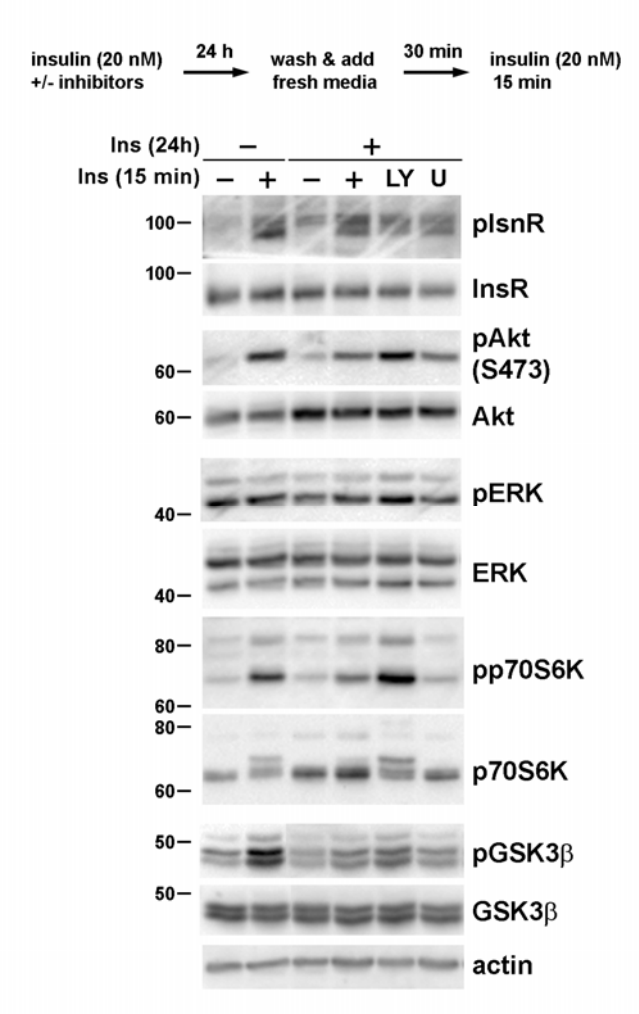

Figure 17. Chronic insulin stimulation, mimicking hypersinulinemia, down regulates cortical neurons' ability to respond to acute insulin stimulation. The cells were incubated with insulin along with 20 μM LY294002 (LY) or U0126 (U) for 24 h. The cells were washed and incubated in fresh treatment media for 30 min prior to acute insulin stimulation for 15 min. Immunoblotting was performed using the indicated antibodies.

These observations were confirmed in an animal model of type 2 diabetes, the BKS-db/db mouse. At 24 weeks of age (20 weeks of diabetes) cortical slices were harvested from db/db and db^+ treated with 20 nM insulin for 0 -60 min. Insulin stimulation resulted in time-dependent increase in Akt phosphorylation in db+ cortical slices (Fig 18). In contrast, Akt from db/db cortical slices exhibit higher basal phosphorylation and insulin treatment did not further increase this phosphorylation. These results confirm our *in vitro* observations and demonstrate that hyperinsulinemia may induce insulin resistance in cortical neurons as detected by reduced Akt activation in response to further insulin treatment.

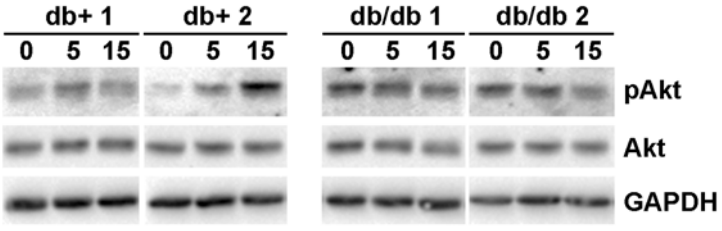

Figure 18. Insulin cannot stimulate Akt phosphorylation in db/db cortex. Cortical slices were harvested from db+ and db/db mice and stimulated with 20 nM insulin. Typical results from two out of 5 animals tested from each group are shown.

Hyperinsulinemia resulting from systemic insulin resistance is characteristic of type 2 diabetes and is also part of the constellation of symptoms associated with metabolic syndrome [32]. Because insulin crosses the blood-brain-barrier, levels are also increased within the CNS.

We hypothesized that increased insulin signaling would result in insulin resistance within the central nervous system and contribute to neuronal damage following ischemia-reperfusion injury. In neurons, the PI-3K/Akt pathway is normally activated by insulin and IGF-I and is essential for translating the protective effects of these ligands [29-31, 34]. In the current study, we found that long term (24 h) exposure to insulin increased Akt activation and severely blunted this response following subsequent short term insulin treatment. Acute Akt signaling was restored when the PI 3-K inhibitor, LY294002, was added with 24 h insulin indicating that hyperstimulation of this pathway is involved in the development of insulin resistance. These observations were confirmed in our well-characterized animal model of type 2 diabetes, the db/db mouse. Cortical neurons harvested from these animals exhibited the same blunted Akt activation following a 15 min exposure to insulin as observed under chronic insulin stimulation *in vitro*.

In summary, our experiments reveal that chronic insulin stimulation *in vitro* and *in vivo* results in a decrease in acute insulin stimulated Akt activation. Experiments are ongoing to determine the role(s) of insulin receptor turnover and the signaling capacity of intracellular substrates responsible for insulin signal transduction. The inability of neurons to respond to circulating growth factors including insulin or IGF-I provides a potential explanation of the increased neuronal damage observed in diabetic human patients following stroke and in animal models of ischemia reperfusion injury.

Plans for the Upcoming Year:

We are currently pursuing a study to phenotype the effects of pioglitazone treatment on type1 and type 2 diabetes. BKS-db/db and db+ mice (BKS.Cg-m +/+ Leprdb/J, JAX Mice stock # 000642) were purchased from Jackson Laboratory (Bar Harbor, ME) and used as a model of type 2 diabetes. Type 1 diabetes was induced by streptozotocin (STZ) injection (150 mg/kg) when db+ mice reached a weight of 20-25 g (~5-7 wk old). The mice will be maintained on a control or pioglitazone chow (Actos mixed in AIN76 chow), receiving 15 mg/kg/day. Mice will be assigned to two sets of six groups, A and B. Group A will be maintained up to 10 wk age, while Group B will be maintained up 20 wk age. Phenotyping will be performed according to the schedule in Table 4.

By activating the nuclear receptor, peroxisome proliferator-activated receptor gamma, pioglitazone regulates the transcription of certain genes that are insulin sensitive. Consequently, studies have shown that pioglitazone lowers triglyceride, insulin, HbA1c and glucose levels in mice with type 2 diabetes.

Within Groups A and B, there are six subgroups: db+ control, db/db (type 2 model), and STZ-injected db+ (type 1 model), each on control or pioglitazone chow. Twelve mice will be assigned to each subgroup (144 mice total).

Throughout this study we will be comparing neuropathy phenotypes and biochemical changes between type 1 and type 2 diabetes with and without pioglitazone treatment. By such comparison we will be able to determine the effects of pioglitazone treatment on the onset and progression of neuropathy. Our goal for Group A is to phenotype the effects of pioglitazone on pain molecules during the onset and progression of painful neuropathy at 10 wk age, including mechanistic profiling of pain pathways in DRG, spinal cord, footpads, and brain. Our goal for Group B is to phenotype the effects of pioglitazone on the progression of neuropathy at 20 wk age by performing terminal neuropathy phenotyping, including exploration of biochemical alterations in DRG, sciatic nerve, spinal cord, and brain. We will also explore all aspects of diabetic nephropathy with our collaborator, Drs. Brosius.

Table 4. Neuropathy Phenotyping Schedule for Group A and Group B

Evaluation	Week 4	Week 8	Week 10	Week 12	Week 16	Week 20
Weight	A, B	A, B	A, B	B	B	B
Fasting Blood Glucose	A, B	A, B	A, B	B	B	B
HbA1C			A			B
Insulin level			A			B
Thermal sensitivity testing	A, B	A, B	A, B	B	B	B
Nerve conductions		B				B
Von Frey mechanical sensation	A, B	A, B	A, B	B	B	B
Intraepidermal nerve fiber density & skin microvessel analysis			A			B
IHC markers			A			B
Tissue Harvest			A			B

2. Collaboration:

We have 3 collaborations with different AMDCC investigators. Our primary collaboration is with Drs. Frank Brosius and Matthias Kretzler, as we continue to phenotype all diabetic nephropathy mouse models for DPN. This productive collaboration has lead to not only a series of publications but also a recently funded R24 application where we will use a systems biology approach to identify potential therapeutic targets in common between the two complications (NIH 1 R24 DK082841-01 09/01/09 - 09/29/14 Integrated Systems Biology Approach to Diabetic Microvascular Complications). The newly planned pioglitazone study will address both complications.

We also collaborate with and phenotype mice for the Smithies group. Our data are in press [35] and we will continue this productive collaboration as appropriate models are generated. We have also gone to the University of Colorado where we phenotyped a large group of animals for Moshe Levi and of interest, while these animals have a nephropathy phenotype, there is no measurable DPN in this cohort.

Finally, we have in place, what we call the “Diabetic Neuropathy Road Show” i.e. we have purchased all needed equipment to easily go to other institutions and phenotype their animals. Thus, for future non-University of Michigan collaborations, investigators can either send the animals to us, or we can travel to the collaborating institution, as we did for Dr. Levi. We anticipate going to JAX laboratories to phenotype animals in the future, as discussed in an AMDCC conference call.

3. Address Previous EAC Comments

NEUROPATHY

Feldman

- *The overall goal of this project is to study the effects of diabetes-mediated oxidative stress on the nervous system. The PI has made tremendous progress towards her proposed goals. She is extremely productive and is at the cutting edge for this field. Her studies of tau phosphorylation are particularly exciting. She has adequately addressed the prior review; one reviewer said the work was too 'sciatic-centric'; she has now 'branched out' so to speak (as evidenced with the brain, aging, and tau studies shown]. The work-to-date is impressive, and the PI is encouraged to keep at it!*

- *Dr. Feldman is strongly encouraged to collaborate with the new AMDCC P&F awardees.*

  We agree with this EAC recommendation and will contact Dr. Dell from Cleveland, only a 3 hour drive from our institution. Her P&F award focuses on novel MRI imaging of kidneys from type 2 murine models to assess diabetic nephropathy. We have a recently funded grant from the JDRF to assess human diabetic neuropathy with MRI imaging. A collaboration, sharing technologies, would of interest to us. We will pursue this within the next 3 months.

- *Overall very good progress. The data on low dose STZ vs. high dose and the anesthesia effects are very useful.*

  We are preparing a manuscript comparing our results with high and low dose STZ animals. Our final data on the differential effects of anesthetics on electrophysiological measurements is provisionally accepted with minor revisions, as discussed in our progress report.

- *The experiments in the diet induced obese B6 mice are interesting, but whether the neuropathic changes can be ascribed to dyslipidemia is questionable, since high fat diet feeding induces numerous changes in B6 mice (eg thousands of genes change expression levels in multiple organ systems after only two weeks of high fat diet feeding).*

  We agree with the EAC and are currently completing Affymetrix analyses of both the sciatic nerves and dorsal root ganglia from these animals. We have a Bioinformatics Ph.D. graduate student rotating in our laboratory in the fall who will begin the bioinformatics analyses of these data under the direction of a new bioinformatics postdoctoral fellow in our laboratory, Dr. Junguk Hur. The data we presented on these animals last year was published in Diabetes and we have written a review on the subject in the Journal of the Peripheral Nervous System. We are very committed to continue to dissect out the role of hyperlipidemia in the pathogenesis of DPN.

- *The data on the influences of diabetes on tau are intriguing. It is premature to draw any conclusions about effects of type 2 vs. type 1 since the described experiments primarily compare BKS to B6, two very different mouse strains. A better strategy to look at type 1 vs. 2 might be to compare BKS-db/db to STZ treated BKS-db/+.*

We cannot thank the EAC enough for this suggestion. We have now completed a large experiment (12 animals per group) comparing both DPN as well as cortical and hippocampal tau cleavage in db+, db+STZ and dbdb at 8, 12 and 20 weeks of age. The full data set are in the process of being analyzed and to our knowledge, this is the first direct comparison of type 2 diabetes and two neurological complications on the same background strain.

- *It is planned to continue studies aimed at exploring the differential influences of dyslipidemia and hyperglycemia on the development of diabetic neuropathy. It is unclear how the comparison of ApoE 3KO, LDLR 3KO and B6 will achieve this. ApoE and LDLR are not equivalent, each gene is inducing its own effects as demonstrated by the different phenotypes of the mice. Wouldn't it be better to have a defined genetic change (ie mutant vs wt allele of the same gene) that induces dyslipidemia as is proposed with the APOE-/-,db/db mice (ie comparing ApoE +/-;db/db against ApoE-/-;db/db)? In the case of the ApoE 3KO and LDLR 3KO it is also stated that both lines develop dyslipidemia.*

  Altering levels of one gene such as ApoE directly addresses the question of the effect of ApoE but does not resolve the question we are most interested in- the role of dyslipidemia in neuropathy. Complete phenotyping of two different models, with careful consideration of the effects of the genes we have deleted- ApoE or Ldlr- will further our understanding of dyslipidemia-mediated mechanisms in the peripheral nervous system. Interim analyses reveal that neuropathy remains present in hyperlipidemic mice when separated from hyperglycemia (the Ldlr 3KO mouse) and may be further distinguished since the particular strain of ApoE mice does not remain hyperglycemic at 20 weeks on the low glycemic diet we selected. We therefore anticipate novel insights into the progression or recovery from neuropathy in the absence of hyperglycemia from these mice that has not previously been accomplished.

  We are close to completing a 24 wk complete neuropathy phenotyping of our triple knockout (3 KO) mice that are deficient in either ApoE or in the low density lipoprotein receptor Ldlr and are both additionally lacking leptin (ob/ob) and apolipoprotein B-48. Once we confirm the degrees of obesity, hyperinsulinemia, hyperlipidemia, hyperglycemia, and neuropathy in the mice, our goal is manipulate the glycemia and/or lipidemia in the mice in order to dissect the contributions of these parameters to the progression of neuropathy. Clinical data have indicated that hypertriglyceridemia is associated with mild or subclinical neuropathy [36-38]. We anticipate that we will be able to demonstrate mild neuropathy caused by hyperlipidemia alone in our mice and, additionally, that both hyperglycemia and hyperlipidemia produce additive effects upon nerve oxidative stress and injury to compound the progression of neuropathy.
  The mice are maintained on the same chow as the original studies [39] the 22/5 Rodent Diet from Harlan Teklad (Indianapolis, IN), containing 22% protein, 5% fat, and 4.5% fiber. We present selected phenotyping data up to 24 wk of age. Plasma samples have been sent to our collaborators at the University of Washington for lipid profiling and insulin measurements. We show modestly accelerated weight gain in the ApoE 3KO mice compared to the Ldlr 3KO mice (Fig. 19, top panels). Weights are similar by 16 wk of age and are maintained up to 24 wk of age. The different glycemia status of the mice is evident by 12 wk of age (Fig 19, middle panels). Ldlr 3KO mice demonstrate only modest increases in fasting blood glucose over the 24 wk while ApoE 3KO mice have significant hyperglycemia from 12- 20 wk. We noted that glycemia was returning to baseline by 24 wk. At 24 wk, glycated hemoglobin (GHb) is significantly increased in

ApoE ob/ob mice compared with their ob/+ littermates, while GHb is only modestly increased in Ldlr ob/ob mice compared with their ob/+ littermates.

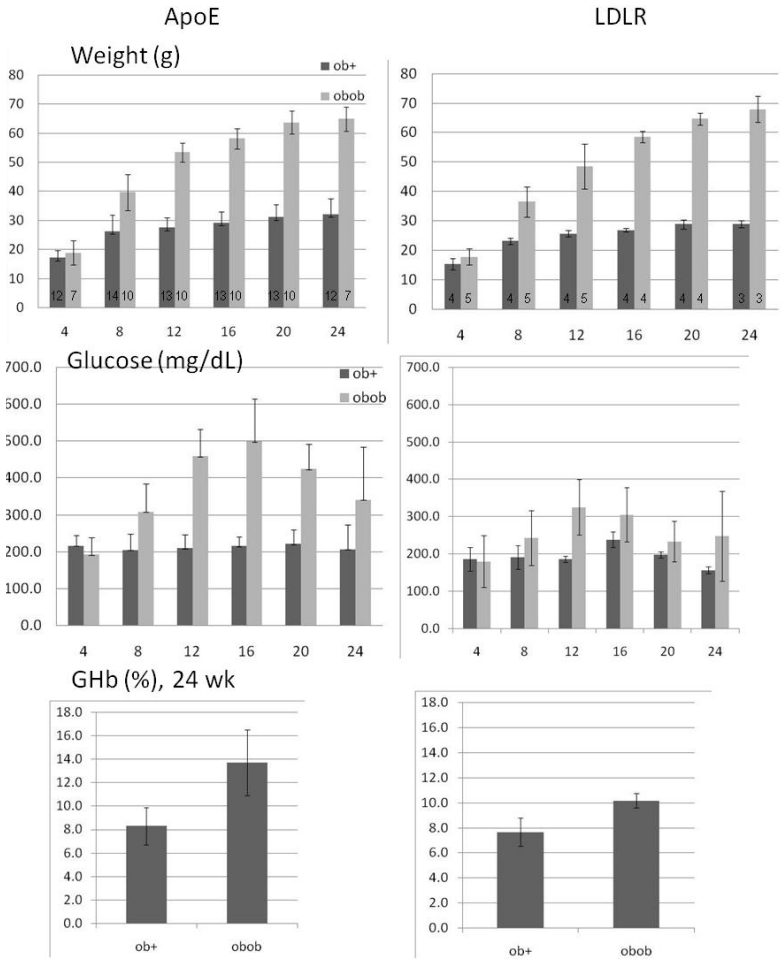

Figure 19. Phenotyping of the 3KO mice. Body weight and fasting (4 h) blood glucose were measured every 4 wk and glycated hemoglobin (GHb) was measured at 24 wk. Bars represent the mean and standard deviation of the data. Numbers at the bottom of the bars represent the number of mice in each group to date.

We have some neuropathy phenotyping data to date, although morphological analyses (nerve morphometry by electron microscopy and intraepidermal nerve fiber density counting) remain to be completed. At 16 wk, there was clearly significantly greater neuropathy in the ApoE 3KO mice when comparing ob/ob to ob/+ littermates or when comparing with Ldlr 3KO mice by Von Frey (Fig. 20 top panels) and hind paw latency (Fig. 20, middle panels). In the ApoE 3KO mice Von Frey and hind paw measures did not change between 16 and 24 wk, but in the Ldlr 3KO mice, both Von Frey and hind paw measures worsened so the neuropathy was similar to the ApoE 3KO mice by 24 wk. Nerve conduction velocities were measured in the mice at 24 wk of age. Sural nerve conduction velocities were modestly lower in ob/ob compared to ob/+ mice of both ApoE and Ldlr knockout mice. Similarly, sciatic nerve conduction velocities were decreased in ob/ob compared to ob+ mice.

When full neuropathy and plasma lipid/glucose/insulin phenotyping is completed within the next 2 months, this preliminary study will be submitted for publication as an introduction to *in vivo* evidence that both dyslipidemia and hyperglycemia contribute to the development of neuropathy. The study demonstrates that the Ldlr 3KO mice, despite modest hyperglycemia, develop neuropathy over a slower time-course than hyperglycemic and hyperlipidemic mice. Complete plasma lipid profiling will provide

clues as to the lipid moieties that may be responsible for peripheral nerve injury and we will use this information to design in vitro experiments to explore lipid (e.g. triglyceride or free fatty acid or cholesterol) induced neuronal, Schwann cell, or microvascular endothelial cell injury.

The drop in plasma glucose in the ApoE 3KO mice after 16 wk of age warrants an important follow-up study. In the next experiments, we will maintain the mice up to 32 wk of age (if possible- we have not determined the life span of these mice; they appear well at 24 wk of age but are extremely obese) and determine whether resolution of hyperglycemia is followed by resolution of behavioral and morphological evidence of neuropathy. In another experiment, we will perform preventive studies using metformin to more tightly regulate glucose in the Ldlr 3KO mice, or a lipid lowering therapy in either 3 KO model, to determine whether we can prevent neuropathy by controlling either glucose or lipids.

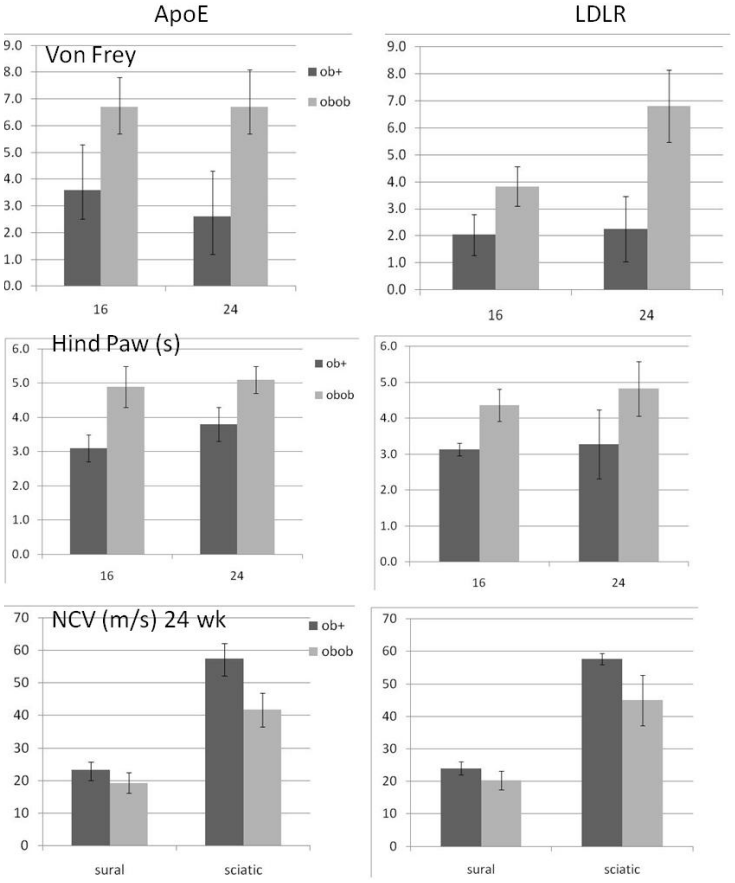

Figure 20. Neuropathy phenotyping in the 3KO mice. Bars represent mean and standard deviation of the mice. Between 3-7 mice are included per group and the final group size will be 6-8 mice, when complete statistical analyses will be performed.

4. Publications:

Vincent A.M., Edwards J.L., McLean L.L., Hong Y., Cerri F., Lopez I., Quattrini A., **Feldman E.L.** Mitochondrial biogenesis and fission in axons in cell culture and animal models of diabetic neuropathy. Acta Neuropathol. 2010 May 15. [Epub ahead of print] PMID: 20473509

Cheng H.T., Dauch J.R., Oh S.S., Hayes J.M., Hong Y., **Feldman E.L.** P38 mediates mechanical allodynia in a mouse model of type 2 diabetes. *Mol Pain.* 6:28, 2010 [Epub ahead of print] PMID: 20482876

Pop-Busui R., Roberts L., Pennathur S., Kretzler M., Brosius F.C., **Feldman E.L.** The management of diabetic neuropathy in CKD. Am J Kidney Dis. 55, 365-85. 2009 PMID: 20042258

Lentz S.I., Edwards J.L., Backus C., McLean L.L., Haines K.M., and **Feldman E.L.** Mitochondrial DNA (mtDNA) Biogenesis: Visualization and Duel Incorporation of BrdU and EdU Into Newly Synthesized mtDNA In Vitro. *J Histochemistry & Cytochemistry* 58, 207–218, 2010 PMID: 19875847

Edwards J.L., Quattrini A., Lentz S.I., Figueroa-Romero C., Cerri F., Backus C., Hong Y., **Feldman E.L**. Diabetes regulates mitochondrial biogenesis and fission in neurons. *Diabetologia* 53, 160-169. 2009 PMID: 19847394

Kim B., Backus C., Oh S.S., Hayes J.M., **Feldman E.L.** Increased Tau Phosphorylation And Cleavage In Mouse Models of Type 1 And Type 2 Diabetes. *Endocrinology* 150, 5294-5301 2009 PMID: 19819959

Currently in press, in revision or submitted:

Kim B., Sullivan K.A., Backus C., **Feldman E.L.** Cortical Neurons Develop Insulin Resistance and Blunted Akt Signaling in Response to a Diabetic Environment. *Antioxid. Redox Signal*, submitted

Oh S.S., Hayes J.M., Sims-Robinson C., Sullivan K.A., **Feldman E.L.** The effects of anesthesia on measures of nerve conduction velocity in male C57Bl6/J mice. *Neurosci Lett* 2010 in revision

REFERENCES

[1] Vincent AM, Edwards JL, McLean LL, Hong Y, Cerri F, Lopez I, Quattrini A, Feldman EL (2010) Mitochondrial biogenesis and fission in axons in cell culture and animal models of diabetic neuropathy. *Acta Neuropathol*.

[2] Lentz SI, Edwards JL, Backus C, McLean LL, Haines KM, Feldman EL (2009) Mitochondrial DNA (mtDNA) Biogenesis: Visualization and Duel Incorporation of BrdU and EdU Into Newly Synthesized mtDNA In Vitro. *J Histochem Cytochem*.

[3] Oh SS, Hayes JM, Sims-Robinson C, Sullivan KA, Feldman EL (2010) The effect of anesthesia on the measures of nereve soncducetion velocity in male C57Bl6/J mice. *Neurosci Lett* **in revision**.

[4] Cheng HT, Dauch JR, Oh SS, Hayes JM, Hong Y, Feldman EL (2010) P38 mediates mechanical allodynia in a mouse model of type 2 diabetes. *Mol Pain* **6**, 28.

[5] Kim B, Sullivan KA, Backus C, Feldman EL (2010) Cortical Neurons Develop Insuin Resistance and Blunted Akt Signaling to a Diabetic Environment. *Antioxid Redox Signal* **submitted**.

[6] Leinninger GM, Backus C, Sastry AM, Yi YB, Wang CW, Feldman EL (2006) Mitochondria in DRG neurons undergo hyperglycemic mediated injury through Bim, Bax and the fission protein Drp1. *Neurobiol Dis* **23**, 11-22.

[7] Vincent AM, Olzmann JA, Brownlee M, Sivitz WI, Russell JW (2004) Uncoupling proteins prevent glucose-induced neuronal oxidative stress and programmed cell death. *Diabetes* **53**, 726-734.

[8] Vincent AM, Russell JW, Sullivan KA, Backus C, Hayes JM, McLean LL, Feldman EL (2007) SOD2 protects neurons from injury in cell culture and animal models of diabetic neuropathy. *Exp Neurol* **208**, 216-227.

[9] Vincent AM, McLean LL, Backus C, Feldman EL (2005) Short-term hyperglycemia produces oxidative damage and apoptosis in neurons. *FASEB J* **19**, 638-640.

[10] Antkowiak B (1999) Different actions of general anesthetics on the firing patterns of neocortical neurons mediated by the GABA(A) receptor. *Anesthesiology* **91**, 500-511.

[11] Antkowiak B (2001) How do general anaesthetics work? *Naturwissenschaften* **88**, 201-213.

[12] Rudolph U, Antkowiak B (2004) Molecular and neuronal substrates for general anaesthetics. *Nat Rev Neurosci* **5**, 709-720.

[13] Roth DM, Swaney JS, Dalton ND, Gilpin EA, Ross J, Jr. (2002) Impact of anesthesia on cardiac function during echocardiography in mice. *Am J Physiol Heart Circ Physiol* **282**, H2134-H2140.

[14] Thompson JS, Brown SA, Khurdayan V, Zeynalzadedan V, Sullivan PG, Scheff SW (2002) Early effects of tribromoethanol, ketamine/xylazine, pentobarbital and isoflurane anesthesia on hepatic and lymphoid tissue in ICR mice. *Comp Med* **52**, 63-67.

[15] Chu DK, Jordan MC, Kim JK, Couto MA, Roos KP (2006) Comparing isoflurane with tribromoethanol anesthesia for echocardiographic phenotyping of transgenic mice. *J Am Assoc Lab Anim Sci* **45**, 8-13.

[16] Zeller W, Meier G, Burki K, Panoussis B (1998) Adverse effects of tribromoethanol as used in the production of transgenic mice. *Lab Anim* **32**, 407-413.

[17] Cheng HT, Dauch JR, Hayes JM, Hong Y, Feldman EL (2009) Nerve growth factor mediates mechanical allodynia in a mouse model of type 2 diabetes. *J Neuropathol Exp Neurol* **68**, 1229-1243.

[18] Ji RR, Gereau RWt, Malcangio M, Strichartz GR (2009) MAP kinase and pain. *Brain Res Rev* **60**, 135-148.

[19] O'Connor AB, Dworkin RH (2009) Treatment of neuropathic pain: an overview of recent guidelines. *Am J Med* **122**, S22-32.

[20] Coulthard LR, White DE, Jones DL, McDermott MF, Burchill SA (2009) p38(MAPK): stress responses from molecular mechanisms to therapeutics. *Trends Mol Med* **15**, 369-379.
[21] Ninomiya JK, L'Italien G, Criqui MH, Whyte JL, Gamst A, Chen RS (2004) Association of the metabolic syndrome with history of myocardial infarction and stroke in the Third National Health and Nutrition Examination Survey. *Circulation* **109**, 42-46.
[22] Kernan WN, Inzucchi SE, Viscoli CM, Brass LM, Bravata DM, Horwitz RI (2002) Insulin resistance and risk for stroke. *Neurology* **59**, 809-815.
[23] McNeill AM, Rosamond WD, Girman CJ, Golden SH, Schmidt MI, East HE, Ballantyne CM, Heiss G (2005) The metabolic syndrome and 11-year risk of incident cardiovascular disease in the atherosclerosis risk in communities study. *Diabetes Care* **28**, 385-390.
[24] Dekker JM, Girman C, Rhodes T, Nijpels G, Stehouwer CD, Bouter LM, Heine RJ (2005) Metabolic syndrome and 10-year cardiovascular disease risk in the Hoorn Study. *Circulation* **112**, 666-673.
[25] Harmsen P, Lappas G, Rosengren A, Wilhelmsen L (2006) Long-term risk factors for stroke: twenty-eight years of follow-up of 7457 middle-aged men in Goteborg, Sweden. *Stroke* **37**, 1663-1667.
[26] Hu G, Jousilahti P, Sarti C, Antikainen R, Tuomilehto J (2006) The effect of diabetes and stroke at baseline and during follow-up on stroke mortality. *Diabetologia* **49**, 2309-2316.
[27] Zhao H, Sapolsky RM, Steinberg GK (2006) Phosphoinositide-3-kinase/akt survival signal pathways are implicated in neuronal survival after stroke. *Mol Neurobiol* **34**, 249-270.
[28] Aberg D (2010) Role of the Growth Hormone/Insulin-Like Growth Factor 1 Axis in Neurogenesis. *Endocr Dev* **17**, 63-76.
[29] Duarte AI, Santos P, Oliveira CR, Santos MS, Rego AC (2008) Insulin neuroprotection against oxidative stress is mediated by Akt and GSK-3beta signaling pathways and changes in protein expression. *Biochim Biophys Acta* **1783**, 994-1002.
[30] Sanderson TH, Kumar R, Murariu-Dobrin AC, Page AB, Krause GS, Sullivan JM (2009) Insulin activates the PI3K-Akt survival pathway in vulnerable neurons following global brain ischemia. *Neurol Res* **31**, 947-958.
[31] Willaime-Morawek S, Arbez N, Mariani J, Brugg B (2005) IGF-I protects cortical neurons against ceramide-induced apoptosis via activation of the PI-3K/Akt and ERK pathways; is this protection independent of CREB and Bcl-2? *Brain Res Mol Brain Res* **142**, 97-106.
[32] Bruce KD, Hanson MAThe developmental origins, mechanisms, and implications of metabolic syndrome. *J Nutr* **140**, 648-652.
[33] Group DR (1995) Effect of intensive diabetes management on macrovascular events and risk factors in the Diabetes Control and Complications Trial. *American Journal of Cardiology* **75**, 894-903.
[34] Franke TF (2008) PI3K/Akt: getting it right matters. *Oncogene* **27**, 6473-6488.
[35] Kakoki M, Sullivan KA, Backus C, Hayes JM, Oh SS, Hua K, Gasim AM, Tomita H, Grant R, Nossov SB, Kim HS, Jennette JC, Feldman EL, Smithies O (2010) Lack of both bradykinin B1 and B2 receptors enhances nephropathy, neuropathy, and bone mineral loss in Akita diabetic mice. *Proc Natl Acad Sci U S A*.
[36] Elliott J, Tesfaye S, Chaturvedi N, Gandhi RA, Stevens LK, Emery C, Fuller JH (2009) Large-fiber dysfunction in diabetic peripheral neuropathy is predicted by cardiovascular risk factors. *Diabetes Care* **32**, 1896-1900.
[37] Valensi P, Paries J, Attali JR (2003) Cardiac autonomic neuropathy in diabetic patients: influence of diabetes duration, obesity, and microangiopathic complications--the French multicenter study. *Metabolism* **52**, 815-820.

[38] Drory VE, Groozman GB, Rubinstein A, Korczyn AD (1999) Hypertriglyceridemia may cause a subclinical peripheral neuropathy. *Electromyogr Clin Neurophysiol* **39**, 39-41.
[39] Lloyd DJ, McCormick J, Helmering J, Kim KW, Wang M, Fordstrom P, Kaufman SA, Lindberg RA, Veniant MM (2008) Generation and characterization of two novel mouse models exhibiting the phenotypes of the metabolic syndrome: Apob48-/-Lepob/ob mice devoid of ApoE or Ldlr. *Am J Physiol Endocrinol Metab* **294**, E496-505.